INTERNATIONAL JOURNAL FOR NUMERICAL METHODS IN FLUIDS, VOL. 21, 1087–1107 (1995)

NUMERICAL SOLUTION OF TWO-LAYER, TWO-DIMENSIONAL TIDAL FLOW IN A BOUNDARY-FITTED ORTHOGONAL CURVILINEAR CO-ORDINATE SYSTEM

K. W. CHAU

Department of Civil and Structural Engineering, Hong Kong Polytechnic University, Hung Hom, Kowloon, Hong Kong

AND

H. S. JIN

Institute of Environmental Water Science, Hohai University, Nanjing 210024, People's Republic of China

SUMMARY

A new two-layer, two-dimensional mathematical model employing a finite difference method based on numerically generated boundary-fitted orthogonal co-ordinates and a grid 'block' technique for unsteady boundary problems is developed which can be used to simulate flows with density stratification in a natural water-body with complicated topography. In the model the turbulent exchange across the interface is treated empirically and a time-splitting finite difference method with two fractional steps is employed to solve the governing equations. The model is calibrated and verified by comparing the computational results with data measured in Tolo Harbour, Hong Kong. The simulation results mimic the field measurements very closely. The computation shows that the model reproduces the two-layer, two-dimensional tidal flow with density stratification in Tolo Harbour very well. The computed velocity hodographs show that the tidal circulations at various positions in each layer have different patterns and that the features of the patterns are independent of the tidal type except for their scales. The computed Lagrangian pathlines show that the tidal excursion is dependent on the tidal type, especially in the inner harbour and side-coves.

KEY WORDS: two-layer; finite difference; time splitting; orthogonal curvilinear co-ordinates; grid 'block'

1. INTRODUCTION

Generally fluid flows in natural water-bodies need to be described three-dimensionally, especially those in reservoirs, estuaries, bays, coastal areas and so on which are commonly effected by density stratification resulting from salt-water intrusion, temperature difference, etc. Although reliable 3D hydrodynamic models may be available, difficulties are still encountered in most practical engineering problems. One difficulty is the intensive and expensive computational effort required, especially for long-term simulations; for example, the Chesapeake Bay hydrodynamic code[1] was run on a supercomputer. Fortunately, in some cases the density stratification is non-linear, showing an obviously lighter surface layer and a definite mesolimnion. Such a situation may be considered as a two-layer system[2,3] in which a lighter layer flows on a heavier lower layer. In this case the flow features can be considered vertically homogeneous in each layer and can be described in a layer-averaged two-dimensional domain, just as in the depth-averaged model which has proved to be effective for the flow of a homogeneous fluid over the whole depth,[4,5] except at the interface between the two layers.

CCC 0271–2091/95/111087–21

Received September 1994
Revised April 1995

Two-layer flows have been much studied during the past two decades, especially with regard to the internal wave at the interface and its stability[2,3,6,7] and the turbulent exchange across the interface.[8] Several numerical models such as the two-layer segment model[9] and the salt-water intrusion model[10,11] have been developed.

In the numerical modelling of fluid flow, several partial differential equations must be solved numerically within a field. The numerical solution of these partial differential equations requires various discretizations of the region into collections of points or elemental grids. However, the planar feature of a natural water-body is generally complicated, its boundaries are irregular, it may include bends, shallows, sand-bars, etc. and the length–width ratio may be very large. In the finite difference method the use of a rectangular grid system to represent irregular boundaries requires approximations that may introduce large errors and may also result in numerical stability problems.[12] Recent developments in numerical grid generation techniques,[13] however, make it possible to apply general finite difference schemes to areas with complicated boundaries.

Furthermore, the boundaries of natural water-bodies vary gradually with fluctuations of tide or flood, i.e. the boundaries are unsteady.

In this paper a new two-layer, two-dimensional mathematical model employing the finite difference method is developed with the aim of simulating flows with density stratification in a natural water-body with complicated topography. For this purpose the present model utilizes boundary-fitted orthogonal co-ordinates that afford the capability of accurately simulating general flows with irregular boundaries. A grid 'block' technique[14] is employed to tackle the unsteady boundary problem. The governing equations are derived first, followed by the explanation of some special terms and the presentation of the numerical method. The model is then applied to simulate the tidal flow in a real bay—Tolo Harbour, Hong Kong—and is calibrated and verified by comparing the computational results of tidal elevation and velocity with field data. In addition, the computational results have been used to investigate the tidal circulation features in the harbour.

2. DESCRIPTION OF THE GOVERNING EQUATIONS

2.1. Governing equations for two-layer-averaged flow

The model is based on the partial differential equations describing the conservation of mass and momentum of an incompressible fluid over the depth of each layer or over the total depth in areas too shallow for a two-layer representation. In shallow areas in which the position of the interface between the upper (surface) and lower (bottom) layers is equal to or lower than that of the bed, the bottom layer vanishes and only the surface layer will be used, just as in a depth-averaged model.

The hydrodynamic equations solved in this model, apart from the interaction between the layers, are similar to and derived in a similar way to the depth-averaged equations,[4,5] i.e. by integrating the three-dimensional equations vertically from the bottom to the top face of each layer with consideration of the mass and momentum exchange between the layers. A hydrostatic pressure distribution is assumed in each layer, i.e. the convection and friction terms in the momentum equation of the vertical direction are much smaller than the pressure gradient and gravitation. In addition, the Boussinesq approximation is employed, i.e. effects due to variations in density are considered only in terms of gravitation. When using boundary-fitted orthogonal curvilinear grids, the governing equations must be expressed so as to adapt to the orthogonal curvilinear co-ordinate system (ξ, η). They are derived from the three-dimensional equations for incompressible turbulent flow in general orthogonal co-ordinates. A unified orthogonal co-ordinate system is used for both the surface and bottom layers.

In the following discussions the position of the interface is at $z = Z_0$, where z is the vertical co-ordinate and is positive in the upward direction. Figure 1 shows a profile of the two-layer system.

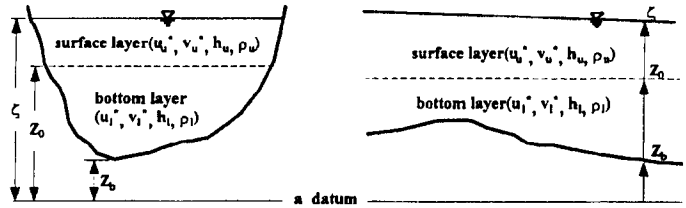

(a) Transverse section (b) Longitudinal profile

Figure 1. Profile of two-layer system

$Z_0 = \text{const.}$ except when $Z_0 = Z_b \neq \text{const.}$ in the shallow areas (Z_b is the bed elevation), i.e. the condition ($\partial Z_0/\partial\xi = 0$ and $\partial Z_0/\partial\eta = 0$) or $Z_0 - Z_b = 0$ will always be obeyed. The vertical distribution of density in each layer is assumed to be constant, i.e. $\rho_u = \rho_u(\xi, \eta)$ and $\rho_l = \rho_l(\xi, \eta)$, where ρ_u and ρ_l indicate the densities of water in the surface and bottom layers respectively and vary horizontally. The pressure at the surface (atmospheric pressure) is also assumed to be constant.

For all variables in this paper, subscripts 'u' and 'l' refer to values in the upper and lower layers respectively; subscripts '0', 's' and 'b' denote values at the interface between the upper and lower layers, at the free surface and at the bed respectively. We define the layer-averaged variables as follows. In the upper layer,

$$\overline{u_u^*}(t,\xi,\eta) = \frac{1}{\zeta - Z_0}\int_{Z_0}^{\zeta} u^*(t,\xi,\eta,z)\,dz, \qquad \overline{v_u^*}(t,\xi,\eta) = \frac{1}{\zeta - Z_0}\int_{Z_0}^{\zeta} v^*(t,\xi,\eta,z)\,dz,$$

$$\int_{Z_0}^{\zeta} u^{*2}dz = (\zeta - Z_0)\overline{u_u^*}^2 + \int_{Z_0}^{\zeta} u_u^{*\prime 2}dz, \qquad \int_{Z_0}^{\zeta} v^{*2}dz = (\zeta - Z_0)\overline{v_u^*}^2 + \int_{Z_0}^{\zeta} v_u^{*\prime 2}dz, \tag{1a}$$

$$\int_{Z_0}^{\zeta} u^* v^* dz = (\zeta - Z_0)\overline{u_u^*}\,\overline{v_u^*} + \int_{Z_0}^{\zeta} u_u^{*\prime} v_u^{*\prime} dz, \qquad u_u^{*\prime} = u^* - \overline{u_u^*}, \qquad v_u^{*\prime} = v^* - \overline{v_u^*},$$

where u^* and v^* are the ξ- and η-components of velocity in the 3D orthogonal curvilinear co-ordinate system respectively. The horizontal acceleration terms in the three-dimensional equations based upon the orthogonal curvilinear co-ordinate system will be integrated as

$$\int_{Z_0}^{\zeta} \frac{\partial u^*}{\partial t}\,dz = \frac{\partial}{\partial t}\int_{Z_0}^{\zeta} u^*\,dz - (u^*)_{z=\zeta}\frac{\partial \zeta}{\partial t} + (u^*)_{z=Z_0}\frac{\partial Z_0}{\partial t}, \tag{1b}$$

$$\int_{Z_0}^{\zeta} \frac{\partial v^*}{\partial t}\,dz = \frac{\partial}{\partial t}\int_{Z_0}^{\zeta} v^*\,dz - (v^*)_{z=\zeta}\frac{\partial \zeta}{\partial t} + (v^*)_{z=Z_0}\frac{\partial Z_0}{\partial t}, \tag{1c}$$

$$\int_{Z_0}^{\zeta} \frac{1}{g_{11}g_{22}}\frac{\partial(g_{22}u^{*2})}{\partial\xi}\,dz = \frac{1}{g_{11}g_{22}}\left[\frac{\partial}{\partial\xi}\left(g_{22}\int_{Z_0}^{\zeta} u^{*2}dz\right) - (g_{22}u^{*2})_{z=\zeta}\frac{\partial\zeta}{\partial\xi} + (g_{22}u^{*2})_{z=Z_0}\frac{\partial Z_0}{\partial\xi}\right], \tag{1d}$$

$$\int_{Z_0}^{\zeta} \frac{1}{g_{11}g_{22}}\frac{\partial(g_{11}u^*v^*)}{\partial\eta}\,dz = \frac{1}{g_{11}g_{22}}\left[\frac{\partial}{\partial\eta}\left(g_{11}\int_{Z_0}^{\zeta} u^*v^*dz\right) - (g_{11}u^*v^*)_{z=\zeta}\frac{\partial\zeta}{\partial\eta} + (g_{11}u^*v^*)_{z=Z_0}\frac{\partial Z_0}{\partial\eta}\right], \tag{1e}$$

$$\int_{Z_0}^{\zeta} \frac{1}{g_{11}g_{22}} \frac{\partial(g_{22}u^*v^*)}{\partial\xi}\,dz = \frac{1}{g_{11}g_{22}}\left[\frac{\partial}{\partial\xi}\left(g_{22}\int_{Z_0}^{\zeta} u^*v^*\,dz\right) - (g_{22}u^*v^*)_{z=\zeta}\frac{\partial\zeta}{\partial\xi} + (g_{22}u^*v^*)_{z=Z_0}\frac{\partial Z_0}{\partial\xi}\right], \tag{1f}$$

$$\int_{Z_0}^{\zeta} \frac{1}{g_{11}g_{22}} \frac{\partial(g_{11}v^{*2})}{\partial\eta}\,dz = \frac{1}{g_{11}g_{22}}\left[\frac{\partial}{\partial\eta}\left(g_{11}\int_{Z_0}^{\zeta} v^{*2}dz\right) - (g_{11}v^{*2})_{z=\zeta}\frac{\partial\zeta}{\partial\eta} + (g_{11}v^{*2})_{z=Z_0}\frac{\partial Z_0}{\partial\eta}\right], \tag{1g}$$

$$\int_{Z_0}^{\zeta} \frac{\partial(u^*w)}{\partial z}\,dz = (u^*w)_{z=\zeta} - (u^*w)_{z=Z_0}, \qquad \int_{Z_0}^{\zeta} \frac{\partial(v^*w)}{\partial z}\,dz = (v^*w)_{z=\zeta} - (v^*w)_{z=Z_0}. \tag{1h}$$

At the free surface, $z=\zeta(t, \xi, \eta)$; differentiating this in time, we can obtain the boundary condition at the water surface as

$$(w)_{z=\zeta} = \left(\frac{Dz}{Dt}\right)_{z=\zeta} = \left(\frac{\partial\zeta}{\partial t} + \frac{u^*}{g_{11}}\frac{\partial\zeta}{\partial\xi} + \frac{v^*}{g_{22}}\frac{\partial\zeta}{\partial\eta}\right)_{z=\zeta}. \tag{1i}$$

In the lower layer,

$$\overline{u_1^*}(t, \xi, \eta) = \frac{1}{Z_0 - Z_b}\int_{Zb}^{Z_0} u^*(t, \xi, \eta, z)\,dz, \qquad \overline{v_1^*}(t, \xi, \eta) = \frac{1}{Z_0 - Z_b}\int_{Zb}^{Z_0} v^*(t, \xi, \eta, z)\,dz,$$

$$\int_{Z_b}^{Z_0} u^{*2}\,dz = (Z_0 - Z_b)\overline{u_1^*}^2 + \int_{Z_b}^{Z_0} u_1^{*\prime 2}dz, \qquad \int_{Z_b}^{Z_0} v^{*2}\,dz = (Z_0 - Z_b)\overline{v_1^*}^2 + \int_{Z_b}^{Z_0} v_1^{*\prime 2}dz, \tag{2a}$$

$$\int_{Z_b}^{Z_0} u^*v^*\,dz = (Z_0 - Z_b)\overline{u_1^*}\,\overline{v_1^*} + \int_{Z_b}^{Z_0} u_1^{*\prime}v_1^{*\prime}dz, \qquad u_1^{*\prime} = u^* - \overline{u_1^*}, \qquad v_1^{*\prime} = v^* - \overline{v_1^*}.$$

The horizontal acceleration terms are

$$\int_{Z_b}^{Z_0} \frac{\partial u^*}{\partial t}\,dz = \frac{\partial}{\partial t}\int_{Z_b}^{Z_0} u^*\,dz - (u^*)_{z=Z_0}\frac{\partial Z_0}{\partial t} + (u^*)_{z=Z_b}\frac{\partial Z_b}{\partial t}, \tag{2b}$$

$$\int_{Z_b}^{Z_0} \frac{\partial v^*}{\partial t}\,dz = \frac{\partial}{\partial t}\int_{Z_b}^{Z_0} v^*\,dz - (v^*)_{z=Z_0}\frac{\partial Z_0}{\partial t} + (v^*)_{z=Z_b}\frac{\partial Z_b}{\partial t}, \tag{2c}$$

$$\int_{Z_b}^{Z_0} \frac{1}{g_{11}g_{22}} \frac{\partial(g_{22}u^{*2})}{\partial\xi}\,dz = \frac{1}{g_{11}g_{22}}\left[\frac{\partial}{\partial\xi}\left(g_{22}\int_{Z_b}^{Z_0} u^{*2}\,dz\right) - (g_{22}u^{*2})_{z=Z_0}\frac{\partial Z_0}{\partial\xi} + (g_{22}u^{*2})_{z=Z_b}\frac{\partial Z_b}{\partial\xi}\right], \tag{2d}$$

$$\int_{Z_b}^{Z_0} \frac{1}{g_{11}g_{22}} \frac{\partial(g_{11}u^*v^*)}{\partial\eta}\,dz = \frac{1}{g_{11}g_{22}}\left[\frac{\partial}{\partial\eta}\left(g_{11}\int_{Z_b}^{Z_0} u^*v^*dz\right) - (g_{11}u^*v^*)_{z=Z_0}\frac{\partial Z_0}{\partial\eta} + (g_{11}u^*v^*)_{z=Z_b}\frac{\partial Z_b}{\partial\eta}\right], \tag{2e}$$

$$\int_{Z_b}^{Z_0} \frac{1}{g_{11}g_{22}} \frac{\partial(g_{22}u^*v^*)}{\partial\xi}\,dz = \frac{1}{g_{11}g_{22}}\left[\frac{\partial}{\partial\xi}\left(g_{22}\int_{Z_b}^{Z_0} u^*v^*dz\right) - (g_{22}u^*v^*)_{z=Z_0}\frac{\partial Z_0}{\partial\xi} + (g_{22}u^*v^*)_{z=Z_b}\frac{\partial Z_b}{\partial\xi}\right], \tag{2f}$$

$$\int_{Z_b}^{Z_0} \frac{1}{g_{11}g_{22}} \frac{\partial(g_{11}v^{*2})}{\partial\eta}\,dz = \frac{1}{g_{11}g_{22}}\left[\frac{\partial}{\partial\eta}\left(g_{11}\int_{Z_b}^{Z_0} v^{*2}\,dz\right) - (g_{11}v^{*2})_{z=Z_0}\frac{\partial Z_0}{\partial\eta} + (g_{11}v^{*2})_{z=Z_b}\frac{\partial Z_b}{\partial\eta}\right], \tag{2g}$$

$$\int_{Z_b}^{Z_0} \frac{\partial(u^* w)}{\partial z}\,\mathrm{d}z = (u^* w)_{z=Z_0} - (u^* w)_{z=Z_b}, \qquad \int_{Z_b}^{Z_0} \frac{\partial(v^* w)}{\partial z}\,\mathrm{d}z = (v^* w)_{z=Z_0} - (v^* w)_{z=Z_b}. \tag{2h}$$

At the bed, $z = Z_b(\xi, \eta)$; we can obtain the boundary condition at the bottom face as

$$(w)_{z=Z_b} = \left(\frac{\mathrm{D}z}{\mathrm{D}t}\right)_{z=Z_b} = \left(\frac{u^*}{g_{11}}\frac{\partial Z_b}{\partial \xi} + \frac{v^*}{g_{22}}\frac{\partial Z_b}{\partial \eta}\right)_{z=Z_b}. \tag{2i}$$

In the subsequent discussions (except those about the dispersion terms) the overbars on all layer-averaged variables have been omitted for the sake of simplicity.

In the surface layer the vertical momentum equation is reduced to

$$p = p_s + \rho_u g(\zeta - z), \quad p_s = \text{const.}, \quad Z_0 \leqslant z \leqslant \zeta. \tag{3}$$

Thus

$$\int_{Z_0}^{\zeta} \frac{1}{\rho_u g_{11}}\frac{\partial p}{\partial \xi}\mathrm{d}z = \frac{h_u g}{g_{11}}\frac{\partial \zeta}{\partial \xi} + \frac{h_u^2 g}{2\rho_u g_{11}}\frac{\partial \rho_u}{\partial \xi}, \qquad \int_{Z_0}^{\zeta} \frac{1}{\rho_u g_{22}}\frac{\partial p}{\partial \eta}\mathrm{d}z = \frac{h_u g}{g_{22}}\frac{\partial \zeta}{\partial \eta} + \frac{h_u^2 g}{2\rho_u g_{22}}\frac{\partial \rho_u}{\partial \eta}.$$

Combining these with equations (1a)–(1h), the free surface boundary condition and the definition of the interface, the layer-averaged continuity and momentum equations are derived as

$$\frac{\partial \zeta}{\partial t} + \frac{1}{g_{11}g_{22}}\left(\frac{\partial(g_{22}h_u u_u^*)}{\partial \xi} + \frac{\partial(g_{22}h_u v_u^*)}{\partial \eta}\right) - w_0 = 0, \tag{4}$$

$$\begin{aligned}
&\frac{\partial(h_u u_u^*)}{\partial t} + \frac{1}{g_{11}g_{22}}\left(\frac{\partial(g_{22}h_u u_u^{*2})}{\partial \xi} + \frac{\partial(g_{11}h_u u_u^* v_u^*)}{\partial \eta}\right) + \frac{h_u u_u^* v_u^*}{g_{11}g_{22}}\frac{\partial g_{11}}{\partial \eta} - \frac{h_u v_u^{*2}}{g_{11}g_{22}}\frac{\partial g_{22}}{\partial \xi} - w_0 u_0^* \\
&\quad = -\frac{h_u g}{g_{11}}\frac{\partial \zeta}{\partial \xi} - \frac{h_u^2 g}{2\rho_u g_{11}}\frac{\partial \rho_u}{\partial \xi} + \frac{1}{g_{11}g_{22}}\left(\frac{\partial(h_u g_{22}\sigma_{1u})}{\partial \xi} + \frac{\partial(h_u g_{11}\tau_{21u})}{\partial \eta}\right) \\
&\qquad + \frac{h_u \tau_{12u}}{g_{11}g_{22}}\frac{\partial g_{11}}{\partial \eta} - \frac{h_u \sigma_{2u}}{g_{11}g_{22}}\frac{\partial g_{22}}{\partial \xi} + \frac{\tau_{s\xi} - \tau_{0\xi}}{\rho} + f h_u v_u^*,
\end{aligned} \tag{5}$$

$$\begin{aligned}
&\frac{\partial(h_u v_u^*)}{\partial t} + \frac{1}{g_{11}g_{22}}\left(\frac{\partial(g_{22}h_u u_u^* v_u^*)}{\partial \xi} + \frac{\partial(g_{11}h_u v_u^{*2})}{\partial \eta}\right) + \frac{h_u u_u^* v_u^*}{g_{11}g_{22}}\frac{\partial g_{22}}{\partial \xi} - \frac{h_u u_u^{*2}}{g_{11}g_{22}}\frac{\partial g_{11}}{\partial \eta} - w_0 v_0^* \\
&\quad = -\frac{h_u g}{g_{22}}\frac{\partial \zeta}{\partial \eta} - \frac{h_u^2 g}{2\rho_u g_{22}}\frac{\partial \rho_u}{\partial \eta} + \frac{1}{g_{11}g_{22}}\left(\frac{\partial(h_u g_{22}\tau_{12u})}{\partial \xi} + \frac{\partial(h_u g_{11}\sigma_{2u})}{\partial \eta}\right) \\
&\qquad + \frac{h_u \tau_{21u}}{g_{11}g_{22}}\frac{\partial g_{22}}{\partial \xi} - \frac{h_u \sigma_{1u}}{g_{11}g_{22}}\frac{\partial g_{11}}{\partial \eta} + \frac{\tau_{s\eta} - \tau_{0\eta}}{\rho} - f h_u u_u^*.
\end{aligned} \tag{6}$$

Similarly, in the bottom layer the vertical momentum equation is approximately expressed as

$$p = p_s + \rho_u g(\zeta - Z_0) + \rho_l g(Z_0 - z), \quad Z_b \leqslant z < Z_0. \tag{7}$$

Thus

$$\int_{Z_b}^{Z_0} \frac{1}{\rho_l g_{11}}\frac{\partial p}{\partial \xi}\mathrm{d}z = \frac{h_l}{\rho_l g_{11}}\left(\rho_u g\frac{\partial \zeta}{\partial \xi} + g h_u \frac{\partial \rho_u}{\partial \xi} + \frac{1}{2} g h_l \frac{\partial \rho_l}{\partial \xi}\right),$$

$$\int_{Z_b}^{Z_0} \frac{1}{\rho_l g_{22}}\frac{\partial p}{\partial \eta}\mathrm{d}z = \frac{h_l}{\rho_l g_{22}}\left(\rho_u g\frac{\partial \zeta}{\partial \eta} + g h_u \frac{\partial \rho_u}{\partial \eta} + \frac{1}{2} g h_l \frac{\partial \rho_l}{\partial \eta}\right).$$

Combining these with equations (2a)–(2h), the bottom boundary condition and the definition of the

interface, the bottom layer-averaged continuity and momentum equations are derived as

$$\frac{1}{g_{11}g_{22}}\left(\frac{\partial(g_{22}h_l u_l^*)}{\partial\xi}+\frac{\partial(g_{11}h_l v_l^*)}{\partial\eta}\right)+w_0=0, \tag{8}$$

$$\begin{aligned}\frac{\partial(h_l u_l^*)}{\partial t}&+\frac{1}{g_{11}g_{22}}\left(\frac{\partial(g_{22}h_l u_l^{*2})}{\partial\xi}+\frac{\partial(g_{11}h_l u_l^* v_l^*)}{\partial\eta}\right)+\frac{h_l u_l^* v_l^*}{g_{11}g_{22}}\frac{\partial g_{11}}{\partial\eta}-\frac{h_l v_l^{*2}}{g_{11}g_{22}}\frac{\partial g_{22}}{\partial\xi}+w_0u_0^*\\&=-\frac{\rho_u g h_l}{\rho_l g_{11}}\frac{\partial\zeta}{\partial\xi}-\frac{g h_l}{\rho_l g_{11}}\left(h_u\frac{\partial\rho_u}{\partial\xi}+\frac{h_l}{2}\frac{\partial\rho_l}{\partial\xi}\right)+\frac{1}{g_{11}g_{22}}\left(\frac{\partial(h_l g_{22}\sigma_{1l})}{\partial\xi}+\frac{\partial(h_l g_{11}\tau_{21l})}{\partial\eta}\right)\\&\quad+\frac{h_l\tau_{12l}}{g_{11}g_{22}}\frac{\partial g_{11}}{\partial\eta}-\frac{h_l\sigma_{2l}}{g_{11}g_{22}}\frac{\partial g_{22}}{\partial\xi}+\frac{\tau_{0\xi}-\tau_{b\xi}}{\rho}+f h_l v_l^*,\end{aligned} \tag{9}$$

$$\begin{aligned}\frac{\partial(h_l v_l^*)}{\partial t}&+\frac{1}{g_{11}g_{22}}\left(\frac{\partial(g_{22}h_l u_l^* v_l^*)}{\partial\xi}+\frac{\partial(g_{11}h_l v_l^{*2})}{\partial\eta}\right)+\frac{h_l u_l^* v_l^*}{g_{11}g_{22}}\frac{\partial g_{22}}{\partial\xi}-\frac{h_l u_l^{*2}}{g_{11}g_{22}}\frac{\partial g_{11}}{\partial\eta}+w_0v_0^*\\&=-\frac{\rho_u g h_l}{\rho_l g_{22}}\frac{\partial\zeta}{\partial\eta}-\frac{g h_l}{\rho_l g_{22}}\left(h_u\frac{\partial\rho_u}{\partial\eta}+\frac{h_l}{2}\frac{\partial\rho_l}{\partial\eta}\right)+\frac{1}{g_{11}g_{22}}\left(\frac{\partial(h_l g_{22}\tau_{12l})}{\partial\xi}+\frac{\partial(h_l g_{11}\sigma_{2l})}{\partial\eta}\right)\\&\quad+\frac{h_l\tau_{21l}}{g_{11}g_{22}}\frac{\partial g_{22}}{\partial\xi}-\frac{h_l\sigma_{1l}}{g_{11}g_{22}}\frac{\partial g_{11}}{\partial\eta}+\frac{\tau_{0\eta}-\tau_{b\eta}}{\rho}-f h_l u_l^*.\end{aligned} \tag{10}$$

Here u_u^*, v_u^* and u_l^*, v_l^* are the ξ- and η-components of layer-averaged velocity in the corresponding layer in the orthogonal curvilinear co-ordinate system respectively, i.e.

$$u_k^*=(u_k x_\xi+v_k y_\xi)/g_{11} \quad\text{and}\quad v_k^*=(u_k x_\eta+v_k y_\eta)/g_{22}, \quad k=\mathrm{u},\mathrm{l}; \tag{11}$$

u_k and v_k are the x- and y-components of layer-averaged velocity in layer k in the Cartesian co-ordinate system respectively; ζ is the water surface level (tidal elevation); h_u and h_l are the water depths in the surface and bottom layers respectively, i.e. $h_u=\zeta-Z_0$ and $h_l=Z_0-Z_b$; u_0^*, v_0^* and w_0 are the ξ-, η- and z-components of velocity at the interface respectively; ρ, g and f are the average density of the water column (herein we take $\rho=(\rho_u+\rho_l)/2$), the gravitational acceleration and the Coriolis coefficient respectively ($g=9{\cdot}81$ m s^{-2}; $f=2\Omega\sin\phi$, where Ω is the angular velocity of the earth's rotation and ϕ is the latitude of the region of interest); $\tau_{s\xi}$, $\tau_{s\eta}$, $\tau_{0\xi}$, $\tau_{0\eta}$ and $\tau_{b\xi}$, $\tau_{b\eta}$ are the ξ- and η-components of shear stress on the water surface, on the interface and on the bottom respectively, which may also include the contribution of horizontal stresses due to the spatial variation of the free surface and the bed elevation; σ_{1u}, σ_{2u}, τ_{12u}, τ_{21u} and σ_{1l}, σ_{2l}, τ_{12l}, τ_{21l} are the layer-averaged effective stresses resulting from turbulence (may also include molecular diffusion and dispersion) in the corresponding layers; g_{11}, g_{22} and J are the orthogonal co-ordinate transformation relationships (a sketch of the co-ordinate transformation is shown in Figure 2) given by

$$g_{11}=\sqrt{(x_\xi^2+y_\xi^2)}, \qquad g_{22}=\sqrt{(x_\eta^2+y_\eta^2)}, \qquad J=x_\xi y_\eta-x_\eta y_\xi=g_{11}g_{22}, \tag{12}$$

$$x_\xi=\frac{\partial x}{\partial\xi}, \qquad x_\eta=\frac{\partial x}{\partial\eta}, \qquad y_\xi=\frac{\partial y}{\partial\xi}, \qquad y_\eta=\frac{\partial y}{\partial\eta}. \tag{13}$$

When integrating the advection terms in the momentum equations vertically from the bottom to the top face of each layer, we have the following additional terms, called dispersion, resulting from the non-uniform velocity distribution along the depth: in the surface layer, corresponding to the left sides of (5) and (6) respectively,

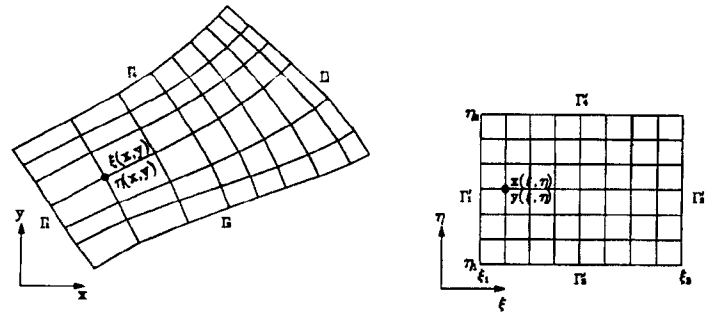

(a) The physical plane (b) The transformed plane

Figure 2. Sketch of co-ordinate transformation

$$-\frac{1}{g_{11}g_{22}}\left(\frac{\partial}{\partial\xi}[g_{22}h_u(\overline{-u_u^{*\prime 2}})]+\frac{\partial}{\partial\eta}[g_{11}h_u(\overline{-u_u^{*\prime}v_u^{*\prime}})]+h_u(\overline{-u_u^{*\prime}v_u^{*\prime}})\frac{\partial g_{11}}{\partial\eta}-h_u(\overline{-v_u^{*\prime 2}})\frac{\partial g_{22}}{\partial\xi}\right)$$

and

$$-\frac{1}{g_{11}g_{22}}\left(\frac{\partial}{\partial\xi}[g_{22}h_u(\overline{-u_u^{*\prime}v_u^{*\prime}})]+\frac{\partial}{\partial\eta}[g_{11}h_u(\overline{-v_u^{*\prime 2}})]+h_u(\overline{-u_u^{*\prime}v_u^{*\prime}})\frac{\partial g_{22}}{\partial\xi}-h_u(\overline{-u_u^{*\prime 2}})\frac{\partial g_{11}}{\partial\eta}\right),$$

where

$$\overline{-u_u^{*\prime 2}}=-\frac{1}{h_u}\int_{Z_0}^{\zeta}u_u^{*\prime 2}\mathrm{d}z,\qquad \overline{-v_u^{*\prime 2}}=\frac{1}{h_u}\int_{Z_0}^{\zeta}v_u^{*\prime 2}\mathrm{d}z,\qquad \overline{-u_u^{*\prime}v_u^{*\prime}}=-\frac{1}{h_u}\int_{Z_0}^{\zeta}u_u^{*\prime}v_u^{*\prime}\mathrm{d}z;$$

in the bottom layer, corresponding to the left sides of (9) and (10) respectively,

$$-\frac{1}{g_{11}g_{22}}\left(\frac{\partial}{\partial\xi}[g_{22}h_l(\overline{-u_l^{*\prime 2}})]+\frac{\partial}{\partial\eta}[g_{11}h_l(\overline{-u_l^{*\prime}v_l^{*\prime}})]+h_l(\overline{-u_l^{*\prime}v_l^{*\prime}})\frac{\partial g_{11}}{\partial\eta}-h_l(\overline{-v_l^{*\prime 2}})\frac{\partial g_{22}}{\partial\xi}\right)$$

and

$$-\frac{1}{g_{11}g_{22}}\left(\frac{\partial}{\partial\xi}[g_{22}h_l(\overline{-u_l^{*\prime}v_l^{*\prime}})]+\frac{\partial}{\partial\eta}[g_{11}h_l(\overline{-v_l^{*\prime 2}})]+h_l(\overline{-u_l^{*\prime}v_l^{*\prime}})\frac{\partial g_{22}}{\partial\xi}-h_l(\overline{-u_l^{*\prime 2}})\frac{\partial g_{11}}{\partial\eta}\right),$$

where

$$\overline{-u_l^{*\prime 2}}=-\frac{1}{h_l}\int_{Z_b}^{Z_0}u_l^{*\prime 2}\mathrm{d}z,\qquad \overline{-v_l^{*\prime 2}}=-\frac{1}{h_l}\int_{Z_b}^{Z_0}v_l^{*\prime 2}\mathrm{d}z,\qquad \overline{-u_l^{*\prime}v_l^{*\prime}}=-\frac{1}{h_l}\int_{Z_b}^{Z_0}u_l^{*\prime}v_l^{*\prime}\mathrm{d}z.$$

All these terms are similar in their form and behaviour to the turbulence stresses (Reynolds stresses), so we count them together with the relevant stresses, i.e. the effective stresses in (5), (6), (9) and (10) represent the composite actions resulting from turbulence and molecular diffusion and dispersion.

2.2. *Some special variables in the governing equations*

2.2.1. Effective stresses. Using the Boussinesq approximation for turbulent stresses,[15] the layer-averaged stresses are expressed as ($k=$ u, l)

$$\sigma_{1k}=2\nu_t\left(\frac{1}{g_{11}}\frac{\partial u_k^*}{\partial\xi}+\frac{\nu_k^*}{J}\frac{\partial g_{11}}{\partial\eta}\right),\tag{14}$$

$$\sigma_{2k} = 2\nu_t\left(\frac{1}{g_{22}}\frac{\partial v_k^*}{\partial \eta} + \frac{u_k^*}{J}\frac{\partial g_{22}}{\partial \xi}\right), \tag{15}$$

$$\tau_{12k} = \tau_{21k} = \nu_t\left(\frac{1}{g_{11}}\frac{\partial v_k^*}{\partial \xi} + \frac{1}{g_{22}}\frac{\partial u_k^*}{\partial \eta} - \frac{u_k^*}{J}\frac{\partial g_{11}}{\partial \eta} - \frac{v_k^*}{J}\frac{\partial g_{22}}{\partial \xi}\right), \tag{16}$$

where ν_t is the effective viscosity coefficient. We make the simple assumption that ν_t maintains a constant distribution in the water column of approximately $\nu_t = \alpha h u_*$, where α is the dimensionless effective viscosity coefficient and u_* is the friction velocity given by $u_* = [C_f(u^{*2} + v^{*2})]^{1/2}$. Here C_f is the resistance coefficient at the bed ($C_f = n^2 g/h^{1/3}$ for the natural situation, where n is the Manning coefficient and $h = (\zeta - Z_b = h_u + h_l)$ is the total depth) and u^* and v^* are the depth-averaged velocity components in the ξ- and η-directions respectively, i.e.

$$u^* = \frac{h_u u_u^* + h_l u_l^*}{h}, \qquad v^* = \frac{h_u v_u^* + h_l v_l^*}{h}. \tag{17}$$

It is possible to employ a more sophisticated turbulence model, e.g. a k–ε turbulence closure or other model,[15–17] instead of the above formula to determine the effective viscosity coefficient ν_t in the new method.

2.2.2. Shear stress on the bed. The bed shear stress is expressed empirically as in the depth-averaged method, except for its direction, according to the velocity components in the bottom layer:

$$\frac{\tau_{b\xi}}{\rho} = C_f(u^{*2} + v^{*2})\frac{u_l^*}{\sqrt{(u_l^{*2} + v_l^{*2})}}, \qquad \frac{\tau_{b\eta}}{\rho} = C_f(u^{*2} + v^{*2})\frac{v_l^*}{\sqrt{(u_l^{*2} + v_l^{*2})}}. \tag{18}$$

2.2.3. Shear stress on the surface. The surface shear stress is assumed to depend only on the wind speed:[18]

$$\tau_{s_\xi} = C_w \rho_a |W| W_\xi, \qquad \tau_{s_\eta} = C_w \rho_a |W| W_\eta, \tag{19}$$

where W_ξ and W_η are the ξ- and η-components of the wind speed W, ρ_a is the density of the air and C_w is the friction coefficient of the wind.

2.2.4. Shear stress on the interface. The shear stress on the interface between the two layers will be represented as

$$\frac{\tau_{0\xi}}{\rho} = \varepsilon_m \frac{\partial u^*}{\partial z} \approx \varepsilon_m \frac{u_u^* - u_l^*}{\delta}, \qquad \frac{\tau_{0\eta}}{\rho} = \varepsilon_m \frac{\partial v^*}{\partial z} \approx \varepsilon_m \frac{v_u^* - v_l^*}{\delta}, \tag{20}$$

where ε_m is the turbulent viscosity coefficient in the vertical direction and δ is the mixing layer thickness at the interface. According to Prandtl's mixing length theory,[15] the turbulent viscosity (ε_{m0}) at the interface for the case without density stratification may be expressed as

$$\varepsilon_{m0} = \left(l_0^2 \left|\frac{\partial u}{\partial z}\right|\right)_{z=Z_0}, \tag{21a}$$

where l_0 is the mixing length and $\partial u/\partial z$ is the vertical gradient of velocity. Here $\partial u/\partial z$ is calculated

approximately from an empirical logarithmic formula of velocity distribution,[15] i.e.

$$\left(\left|\frac{\partial u}{\partial z}\right|\right)_{z=Z_0} \approx \frac{u_*}{\kappa h_1}, \qquad u_* = \sqrt{[C_f(u^{*2}+v^{*2})]}, \qquad \text{hence } \varepsilon_{m0} = l_0^2 \frac{u_*}{\kappa h_1}, \tag{21b}$$

where κ is the von Karman constant, $\kappa \approx 0{\cdot}4$.[15] The mixing length l_0 is generally defined empirically. Here the following empirical non-linear formula, which results in a logarithmic velocity profile under the assumption of a linear shear stress distribution for the whole depth of the column in gradually varying two-dimensional open channel flow, is employed[8] (on the other hand, within the near-bed layer we also get a logarithmic velocity profile under the assumption of a uniform stress distribution and an empirical linear formula for the mixing length):

$$l_0 = \kappa(z - Z_b)\left(1 - \frac{z - Z_b}{h}\right)^{1/2}. \tag{21c}$$

Thus at the interface, i.e. $z = Z_0$, we have

$$l_0 = \kappa h_1\left(1 - \frac{h_1}{h}\right)^{1/2}, \qquad \varepsilon_{m0} = \kappa h_1\left(1 - \frac{h_1}{h}\right)u_*. \tag{21d}$$

Generally ε_m is a function of density stratification. We employ the Richardson number to indicate the stratification degree and use a Munk–Anderson-type empirical formula as follows:

$$\varepsilon_m = \varepsilon_{m0}(1 + \beta Ri)^{\alpha_0}, \tag{22}$$

where β and α_0 are empirical coefficients, $\beta = 10$ and $\alpha_0 = -1/2$;[19] Ri is the gradient Richardson number at the interface and is defined as

$$Ri = -\frac{g}{\rho}\frac{\partial\rho/\partial z}{(\partial u/\partial z)^2} \approx \frac{\rho_l - \rho_u}{\rho}\frac{g\delta}{(u_u^* - u_l^*)^2 + (v_u^* - v_l^*)^2}. \tag{23}$$

On the other hand, it is very difficult to determine the mixing layer thickness δ. Here, in accordance with the definition of mixing length, we let $\delta \approx l_0$ regardless of the effect of density stratification.

In shallow areas the lower layer vanishes and only the surface layer will be used, so the variables with subscript '0' will describe those at the bed, e.g. $\tau_{0\xi} = \tau_{b\xi}$.

2.2.5. Velocities at the interface. In the present model no equation can be used to calculate the horizontal velocity components (u_0^*, v_0^*) at the interface. Because $u_0^* = 0$ and $v_0^* =$ when $h_l = 0$ (i.e. the lower layer vanishes in shallow areas) and it is generally believed that u_0^* lies between u_u^* and u_l^* and that v_0^* lies between v_u^* and v_l^*, u_0^* and v_0^* are calculated approximately by the formulae

$$u_0^* \approx \frac{h_u u_l^* + h_l u_u^*}{h}, \qquad v_0^* \approx \frac{h_u v_l^* + h_l v_u^*}{h}. \tag{24}$$

The vertical velocity (w_0) at the interface, which results in the convective exchange between the upper and lower layers, can be calculated from the layer-averaged continuity equation, i.e. (4) or (8).

2.3. Depth-averaged continuity equation

Combining (4) with (8), we can obtain the following equation for the conservation of mass in the whole depth of the water column;

$$\frac{\partial\zeta}{\partial t} + \frac{1}{g_{11}g_{22}}\left(\frac{\partial[g_{22}(h_u u_u^* + h_l u_l^*)]}{\partial\xi} + \frac{\partial[g_{11}(h_u v_u^* + h_l v_l^*)]}{\partial\eta}\right) = 0. \tag{25}$$

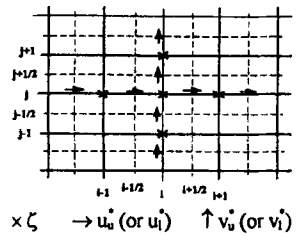

Figure 3. Sketch of node and grid system

This is equivalent to the following depth-averaged continuity equation in the depth-averaged model according to (17):

$$\frac{\partial \zeta}{\partial t}+\frac{1}{g_{11}g_{22}}\left(\frac{\partial(g_{22}hu^*)}{\partial \xi}+\frac{\partial(g_{11}hv^*)}{\partial \eta}\right)=0. \tag{26}$$

3. NUMERICAL METHOD

3.1. Grid system

According to the form of the convection-diffusion equations, a 'staggered' grid system, in which the nodes for velocities and water surface elevation (or pressure, etc.) do not coincide with each other (Figure 3), is set up in the computational domain. In a 'staggered' grid system the discretized continuity equation will include the differences between adjacent velocity components and thus will prevent a wavy velocity field which also satisfies the continuity equation; also, the difference in water surface elevation between two adjacent grid nodes becomes the natural driving force for the velocity component located between those grid nodes.[20]

3.2. Grid 'block' technique

In order to overcome the computational difficulty resulting from the unsteady boundary of the computational domain, a grid 'block' technique[14] is employed in the model. Grid 'block' means that no water will flow out of or into the grid, i.e. the grid is blocked. This technique treats the grid in which the bed elevation is greater than the water surface level as a blocked one by changing the bed roughness, so that the computed velocities at these positions are zero even though these points are included in the computational procedure. The results show that the technique is very effective and the present model is successful in tackling the unsteady computational domain.

3.3. Boundary and initial conditions

To close the above governing equations, boundary conditions are required. There are two types of boundaries: (1) boundaries in the lateral direction, i.e. the side-wall; (2) boundaries in the stream direction, i.e. the upstream and downstream ends and also the confluence of a stream and a tributary.

At the side-wall. Since a boundary-fitted orthogonal co-ordinate system is employed in the present model, the boundary conditions at the side-wall can be treated easily and accurately. The impenetrability condition is specified at the side-wall, i.e. the velocity normal to the side-wall is equal to zero but the tangential velocity is not zero, and when discretizing the momentum equations at the grids near the side-wall, the shear stress on the wall expressed as (16) is replaced by an empirical

formula similar to (18) but using the velocities in the relevant layer. Thus, after linearizing the relevant terms in the momentum equations, the solution of the velocities may be obtained without directly knowing the actual tangential velocity on the boundary.

The water surface elevation (ζ) at the side-wall can be determined by the normal direction momentum equation.

At the upstream and downstream ends. Several types of matched conditions—(a) water surface elevation at both ends, (b) water surface elevation at the upstream end and velocities at the downstream end, (c) velocities at the upstream end and water surface elevation at the downstream end, (d) velocities at both ends—may be specified. Type (c) is preferred in the present model.

At the confluence of a stream and a tributary the velocities are specified exactly , otherwise the boundary must be extended some distance upstream of the tributary to where the velocities or water surface elevation may be determined.

Besides boundary conditions, initial conditions are also required for closing the above unsteady governing equations. However, it is difficult to specify the initial conditions for all the variables in the whole computational domain, e.g. the initial flow field, because plentiful measured data and analytical solutions are not available. In the present model the initial conditions are obtained by interpolating the corresponding boundary conditions at the starting time ($t=0$).

3.4. Numerical scheme

In the orthogonal curvilinear co-ordinate system a general numerical method can be used on condition that the corresponding geometrical features are considered. Here a time-splitting scheme with two fractional steps according to the physical meaning of each term—(1) advection and diffusion, (2) propagation along with source terms—is employed to achieve the numerical solution of the above governing equations.

3.4.1. Advection and diffusion fractional step. In this step the convection and diffusion terms are first separated from the momentum equations (5), (6), (9) and (10), i.e. the following equations are solved ($k=$ u, l):

$$\frac{\partial(h_k u_k^*)}{\partial t}+\frac{1}{g_{11}g_{22}}\left(\frac{\partial(g_{22}h_k u_k^{*2})}{\partial \xi}+\frac{\partial(g_{11}h_k u_k^* v_k^*)}{\partial \eta}\right)$$

$$=\frac{1}{g_{11}g_{22}}\left(\frac{\partial(h_k g_{22}\sigma_{1k})}{\partial \xi}+\frac{\partial(h_k g_{11}\tau_{21k})}{\partial \eta}\right)+\frac{h_k\tau_{12k}}{g_{11}g_{22}}\frac{\partial g_{11}}{\partial \eta}-\frac{h_k\sigma_{2k}}{g_{11}g_{22}}\frac{\partial g_{22}}{\partial \xi}, \tag{27}$$

$$\frac{\partial(h_k v_k^*)}{\partial t}+\frac{1}{g_{11}g_{22}}\left(\frac{\partial(g_{22}h_k u_k^* v_k^*)}{\partial \xi}+\frac{\partial(g_{11}h_k v_k^{*2})}{\partial \eta}\right)$$

$$=\frac{1}{g_{11}g_{22}}\left(\frac{\partial(h_k g_{22}\tau_{12k})}{\partial \xi}+\frac{\partial(h_k g_{11}\sigma_{2k})}{\partial \eta}\right)+\frac{h_k\tau_{21k}}{g_{11}g_{22}}\frac{\partial g_{22}}{\partial \xi}-\frac{h_k\sigma_{1k}}{g_{11}g_{22}}\frac{\partial g_{11}}{\partial \eta}. \tag{28}$$

The time derivatives are discretized by the backward finite difference scheme, the advection terms are discretized by the upwind finite difference scheme and the diffusion terms are discretized by the spatial central finite difference scheme in order to obtain an algebraic equation set for the discrete governing equations. These result in an implicit numerical algorithm. The above equations are all non-linear, so a linearization technique, i.e some variables in the non-linear terms are partially replaced by their

corresponding values at the beginning of this time step (time $= n\Delta t$, where the Δ is the time step used in the computation and the index n denotes the time level of the discretized hydrodynamic variables), is applied when they are discretized. The algebraic equation set is solved iteratively by the tridiagonal matrix algorithm (TDMA), column by column. In this step we obtain the temporal results of velocities ($\tilde{u}_u^*, \tilde{v}_u^*, \tilde{u}_l^*$ and $\tilde{v}_l^*$) which are used in the following propagation step. During this fractional step, no equation for the water surface elevation has to be solved, so it will not vary.

3.4.2. Propagation fractional step. In this step the propagation and other terms (those remaining after the convection and diffusion step) in the momentum equations combined with the continuity equation will be discretized and solved, i.e. the following equations are solved:

$$\frac{\partial(h_u u_u^*)}{\partial t} + \frac{h_u u_u^* v_u^*}{g_{11}g_{22}}\frac{\partial g_{11}}{\partial \eta} - \frac{h_u v_u^{*2}}{g_{11}g_{22}}\frac{\partial g_{22}}{\partial \xi} - w_0 u_0^* = -\frac{h_u g}{g_{11}}\frac{\partial \zeta}{\partial \xi} - \frac{h_u^2 g}{2\rho_u g_{11}}\frac{\partial \rho_u}{\partial \xi} + \frac{\tau_{s\xi} - \tau_{0\xi}}{\rho} + f h_u v_u^*, \quad (29)$$

$$\frac{\partial(h_u v_u^*)}{\partial t} + \frac{h_u u_u^* v_u^*}{g_{11}g_{22}}\frac{\partial g_{22}}{\partial \xi} - \frac{h_u u_u^{*2}}{g_{11}g_{22}}\frac{\partial g_{11}}{\partial \eta} - w_0 v_0^* = -\frac{h_u g}{g_{22}}\frac{\partial \zeta}{\partial \eta} - \frac{h_u^2 g}{2\rho_u g_{22}}\frac{\partial \rho_u}{\partial \eta} + \frac{\tau_{s\eta} - \tau_{0\eta}}{\rho} - f h_u u_u^*, \quad (30)$$

$$\frac{\partial(h_l u_l^*)}{\partial t} + \frac{h_l u_l^* v_l^*}{g_{11}g_{22}}\frac{\partial g_{11}}{\partial \eta} - \frac{h_l v_l^{*2}}{g_{11}g_{22}}\frac{\partial g_{22}}{\partial \xi} + w_0 u_0^*$$

$$= -\frac{\rho_u g h_l}{\rho_l g_{11}}\frac{\partial \zeta}{\partial \xi} - \frac{g h_l}{\rho_l g_{11}}\left(h_u \frac{\partial \rho_u}{\partial \xi} + \frac{h_l}{2}\frac{\partial \rho_l}{\partial \xi}\right) + \frac{\tau_{0\xi} - \tau_{b\xi}}{\rho} = f h_l v_l^*, \quad (31)$$

$$\frac{\partial(h_l v_l^*)}{\partial t} + \frac{h_l u_l^* v_l^*}{g_{11}g_{22}}\frac{\partial g_{22}}{\partial \xi} - \frac{h_l u_l^{*2}}{g_{11}g_{22}}\frac{\partial g_{11}}{\partial \eta} + w_0 v_0^*$$

$$= -\frac{\rho_u g h_l}{\rho_l g_{22}}\frac{\partial \zeta}{\partial \eta} - \frac{g h_l}{\rho_l g_{22}}\left(h_u \frac{\partial \rho_u}{\partial \eta} + \frac{h_l}{2}\frac{\partial \rho_l}{\partial \eta}\right) + \frac{\tau_{0\eta} - \tau_{b\eta}}{\rho} - f h_l u_l^*, \quad (32)$$

together with equation (25).

These equations are also non-linear and a similar linearization technique to that above is employed, but using the results from the convection and diffusion step instead of those at the beginning of this time step. Thus from (29)–(32) we can derive the relationships between $u_u^*, v_u^*, u_l^*, v_l^*$ and ζ at time $(n+1)\Delta t$ as ($k = $ u, l):

$$(u_k^*)_{i+1/2,j}^{n+1} = A_{k,e}^u(\zeta_{i+1,j}^{n+1} - \zeta_{i,j}^{n+1}) + B_{k,e}^u, \qquad (u_k^*)_{i-1/2,j}^{n+1} = A_{k,w}^u(\zeta_{i,j}^{n+1} - \zeta_{i-1,j}^{n+1}) + B_{k,w}^u, \quad (33)$$

$$(v_k^*)_{i,j+1/2}^{n+1} = A_{k,n}^v(\zeta_{i,j+1}^{n+1} - \zeta_{i,j}^{n+1}) + B_{k,n}^v, \qquad (v_k^*)_{i,j-1/2}^{n+1} = A_{k,s}^v(\zeta_{i,j}^{n+1} - \zeta_{i,j-1}^{n+1}) + B_{k,s}^v, \quad (34)$$

where $A_{k,e}^u, B_{k,e}^u, \ldots, A_{k,s}^v, B_{k,s}^v$ are coefficients which can be calculated after the above convection and diffusion fractional step and linearization of some non-linear terms in the equations. In (25) some non-linear terms are linearized as below:

$$h_u u_u^* = (\zeta - Z_0)u_u^* = \zeta^{n+1}\tilde{u}_u^* + (\zeta^n - Z_0)(u_u^*)^{n+1} - \zeta^n \tilde{u}_u^*, \quad (35)$$

$$h_l u_l^* = (Z_0 - Z_b)u_l^* = (Z_0 - Z_b)(u_l^*)^{n+1}, \quad (36)$$

$$h_u v_u^* = (\zeta - Z_0)v_u^* = \zeta^{n+1}\tilde{v}_u^* + (\zeta^n - Z_0)(v_u^*)^{n+1} - \zeta^n \tilde{v}_u^*, \quad (37)$$

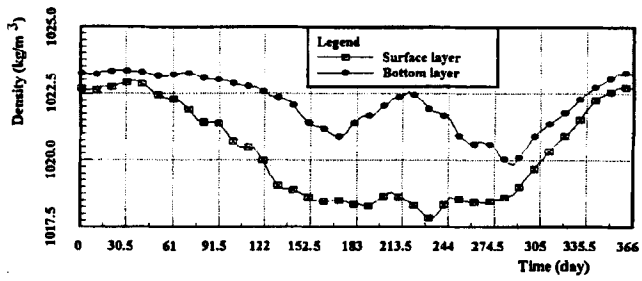

Figure 4. Daily variation in water density at surface and bottom of Tolo Harbour (based on 10 years' measured data during 1981–1990)

$$h_1 v_1^* = (Z_0 - Z_b) v_1^* = (Z_0 - Z_b)(v_1^*)^{n+1}. \tag{38}$$

Discretizing equation (25) with backward time difference and central spatial difference schemes and replacing the corresponding variables and terms by (33)–(38), a linearized algebraic equation set for the water surface elevation (ζ) on the nodes in the computational domain can be established:

$$a_{Pi,j}\zeta_{i,j}^{n+1} = a_{Ei,j}\zeta_{i+1,j}^{n+1} + a_{wi,j}\zeta_{i-1,j}^{n+1} + a_{Ni,j}\zeta_{i,j+1}^{n+1} + a_{Si,j}\zeta_{i,j-1}^{n+1} + b_{i,j}, \tag{39}$$

where $a_{Pi,j}$, $a_{Ei,j}$, $a_{Wi,j}$, $a_{Ni,j}$, $a_{si,j}$ and $b_{i,j}$ are coefficients and i and j are the node numbers in the ξ- and η-directions respectively (Figure 3). Solving the algebraic equation set (39) by the TDMA with alternating direction iteration (ADI), the water surface elevation at time $(n+1)\Delta t$ (ζ^{n+1}) can be obtained. Then the velocities at time $(n+1)\Delta t$ ($(u_u^*)^{n+1}$, $(v_u^*)^{n+1}$, $(u_l^*)^{n+1}$ and $(v_l^*)^{n+1}$) are computed by (33) and (34).

4. APPLICATION IN TOLO HARBOUR, HONG KONG

Tolo Harbour is one of the most valuable natural resources in Hong Kong. It is a nearly land-locked sea inlet with an area of about 52 km^2 and a narrow outlet connecting with Mirs Bay—one of the major south-facing bays in the South China Sea. Its main water-body extends approximately 16 km from south-west at the inner harbour to north-east at the outer channel. The water depth varies from about 2 m in the inner part to over 20 m in the outer part of the Tolo Channel and is about 12 m on average. The average diurnal tidal difference is about 0.97 m, the mean high-tide elevation is 1·75 m and the mean low-tide elevation is 0·78 m (MCD).[21] For most of the year the fresh-water discharged into Tolo Harbour is very little and it can be considered as a bay. However, the differences in surface and bottom water temperature and salinity distributions during the summer can result in density stratification in the vertical water column over the marine waters in Tolo Harbour (see Figure 4), showing an obviously two-layer system. The assumption of homogeneous mixing in existing depth-averaged models such as that developed by Binnie & Partners (Hong Kong)[22] and others, which matches the situation in winter when the strong north-east monsoon causes good turbulent mixing and results in fairly homogeneous water over the vertical water column of the coastal area, will be invalid during the summer season. Nevertheless, it is feasible to develop a two-layer-averaged model to represent the stratification in the vertical water column.

The present model has been applied to Tolo Harbour where the interface position between the surface and bottom layers is located at $Z_0 = -6$ m (MCD), as determined according to some available data measured in Tolo Harbour. Here some results will be reported. For the sake of simplicity the density in each layer is assumed to depend only on time and not to vary horizontally. For future reseach the two-layer flow can be simulated with density variation in both time and space.

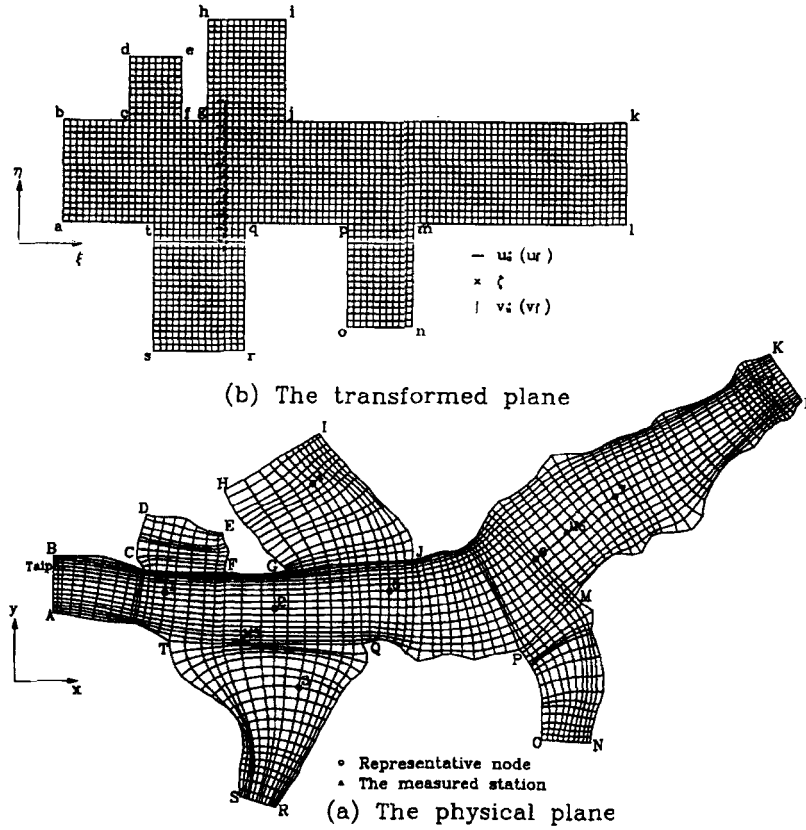

Figure 5. Computational domain and grids

4.1. *Computational domain and boundary and initial conditions*

Tolo Harbour is very irregular in lateral topography and includes several small side-coves. The computational domain is shown in Figure 5(a). The boundary-fitted orthogonal curvilinear grid in the physical plane is displayed in Figure 5(a), while Figure 5(b) shows the corresponding grid in the transformed plane. The orthogonal co-ordinate system in the upper layer is the same as that in the lower layer. A 'staggered' grid system for u_u^*, v_u^* (or u_l^*, v_l^*) and ζ as shown in Figures 3 and 5 is employed.

At the open boundary, i.e. the boundary segment 'KL' (or 'kl' in the transformed plane), a time-varying tidal elevation is specified. The other boundaries are almost all bank boundaries and the impenetrability condition is specified on these boundaries.

The initial conditions can be specified as any value because of the good performance of the model. Here the water surface elevation at each node is taken to be equal to the value at the open boundary at starting time ($t = 0$) and the initial velocities are always taken as zero. The computation shows that any impact of inaccurate initial conditions on the output will soon disappear.

4.2. *Results and analysis*

The time step (Δt) of the model run is set to 5 min, which is far longer than that allowed by the Courant–Friedrichs–Levy (CFL) stability criterion constraint, and the results do not show any

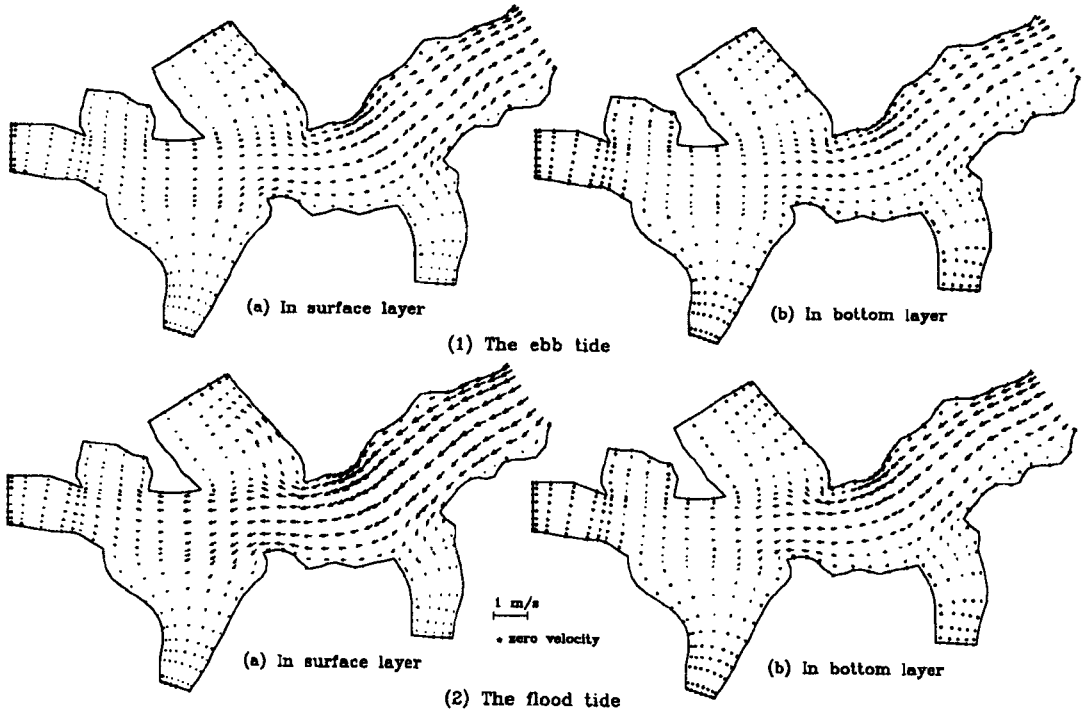

Figure 6. Two-layer flow fields in Tolo Harbour

unreasonable numerical oscillations. The model was calibrated and verified with some available data measured in Tolo Harbour.

Figure 6 shows the flow fields in both the upper and lower layers of ebb and flood tides in Tolo Harbour. The velocities at some positions are zero because the bed elevations at these positions are greater than the water surface level. The flow field results show that the present model can reproduce very well circulations in both layers which are consistent with the topographical features of Tolo Harbour. From these results we also know that the flow directions in the surface and bottom layers may be non-uniform, especially when the current is not too swift.

Figures 7–10 display the computational and measured[23,24] results of tidal elevation and velocity at various stations during 19 August 1978, 9–10 May 1983 and 16–17 May 1983. In Figure 8 a negative velocity denotes a flood tide and a positive velocity denotes an ebb tide. The velocities in Figures 9 and 10 are absolute values. The corresponding computational results of velocity with no density difference between the surface and bottom layers are also shown (as broken curves) for comparison. These three sets of data cover the different tide types: spring tide and neap tide, which are semidiurnal, and mixed tide.

Figures 7, 9(a) and 10(a) show that the tidal elevation at Taipo computed by the present model coincides fairly closely with the measured data in all situations. Figure 8 shows that the model mimics very well the velocity at P2 on 19 August 1978. The measured current at M5 during 9–10 May 1983 and 16–17 May 1983 is available at 2 m depth only; here we compare it with the computational upper-layer-averaged velocity. Although some discrepancies are apparent in Figures 9(b) and 10(b), in general their agreement is still quite good. Figures 8, 9(b) and 10(b) also show that the corresponding computational results of velocity with no density difference between the surface and bottom layers differ considerably from the measured data. The lower-layer velocity is overpredicted and the upper-

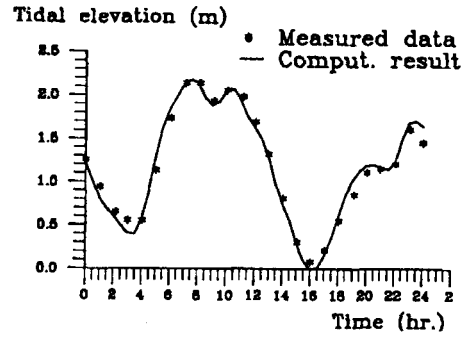

Figure 7. Tidal elevation at Taipo on 19 August 1978

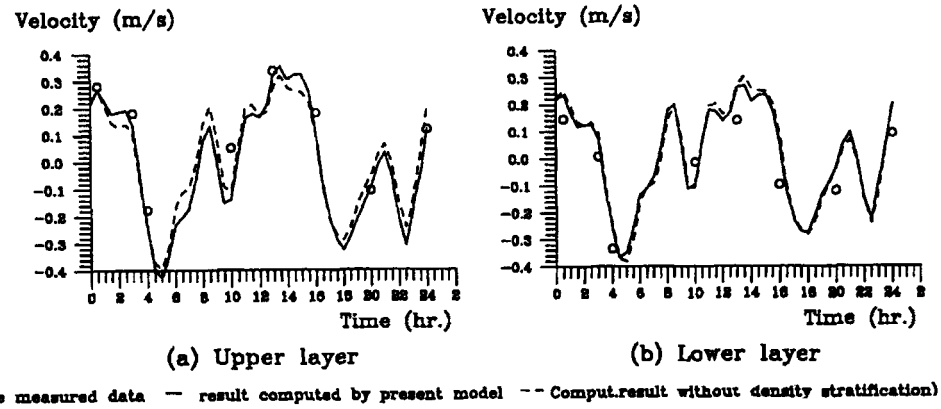

Figure 8. Layer-averaged velocity at P2 along Tolo Channel on 19 August 1978

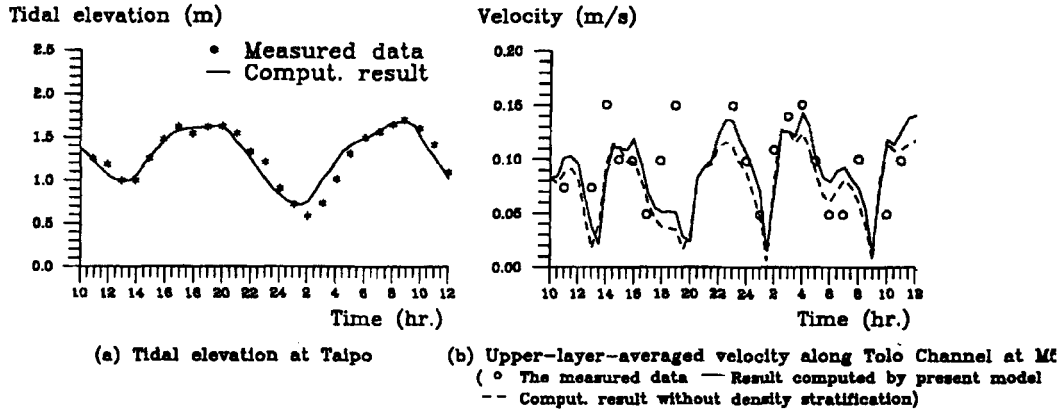

Figure 9. Computational and measured results during 9–10 May 1983

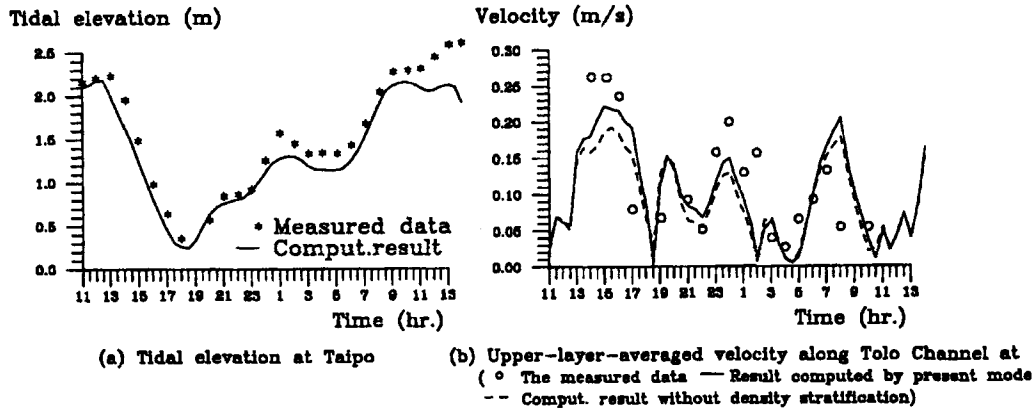

Figure 10. Computational and measured results during 16–17 May 1983 measured results during 16–17 May 1983

layer velocity is underpredicted similarly as with a depth-averaged model. Hence it is proved that the density stratification plays an important role in the tidal circulation and we believe that the present model represents the two-layer, two-dimensional tidal flow in Tolo Harbour very well.

The computed velocity hodographs at 10 different points and the Lagrangian pathlines at five different positions, which are located in various areas of Tolo Harbour and are good representatives of this coastal area, have been used to investigate the flow features in Tolo Harbour. Figures 11–16 show the Lagrangian pathlines and computed velocity hodographs during a 1 day period at representative points corresponding to spring tide, neap tide and mixed tide. The computed velocity hodographs show that the Eulerian velocities in most of the harbour, especially in the outer area, i.e. in the Tolo Channel, have a prevailing direction along the channel and their transverse component is very small relative to their longitudinal counterpart; however, the prevailing directions in the surface layer are generally

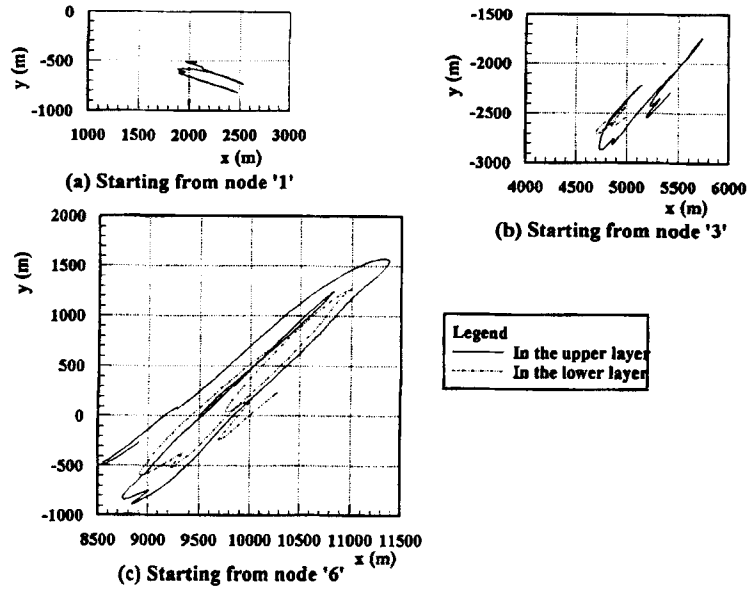

Figure 11. Computed Lagrangian pathlines on 19 August 1978

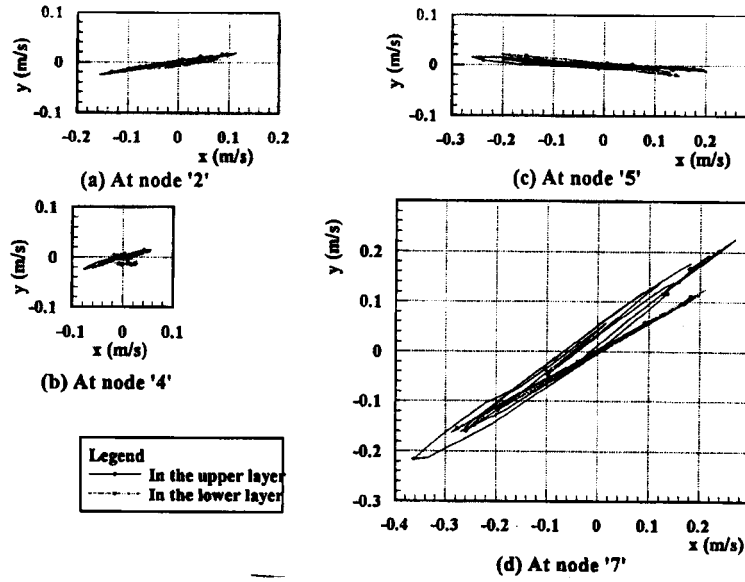

Figure 12. Computed velocity hodographs on 19 August 1978

different from those in the bottom layer. In the inner part 'ABCT' and the three side-coves 'QRST', 'MNOP' and 'GHIJ' we find anticlockwise circulation patterns. A clockwise circulation exists in the cove 'CDEF'. However, in the Tolo Channel and near point '2' clockwise circulations exist in the surface layer and anticlockwise circulations in the bottom layer. Near point '5' the circulation pattern is vague, possibly owing to the side-cove 'GHIJ'. These features of the circulation patterns are independent of the tidal type except for their scales. The computed Lagrangian pathlines show that the tidal excursion is dependent on the tidal type, especially in the inner harbour and side-coves; during neap tide it is very small and this is bad for pollutant transport.

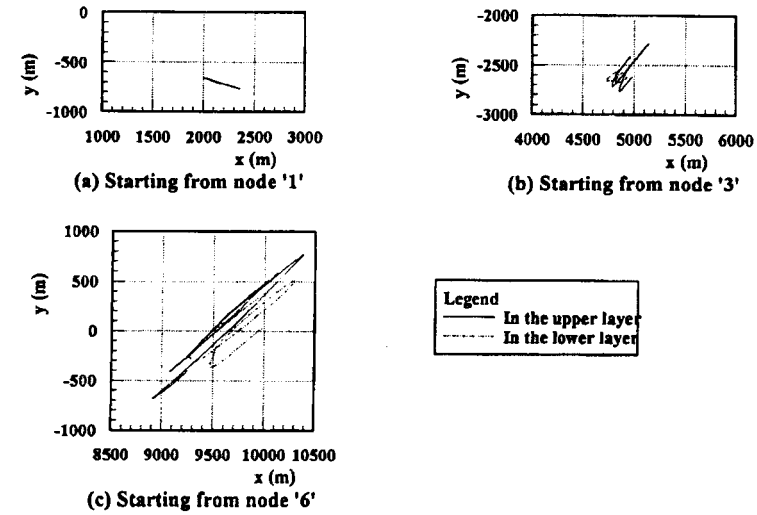

Figure 13. Computed Lagrangian pathlines during 9–10 May 1983

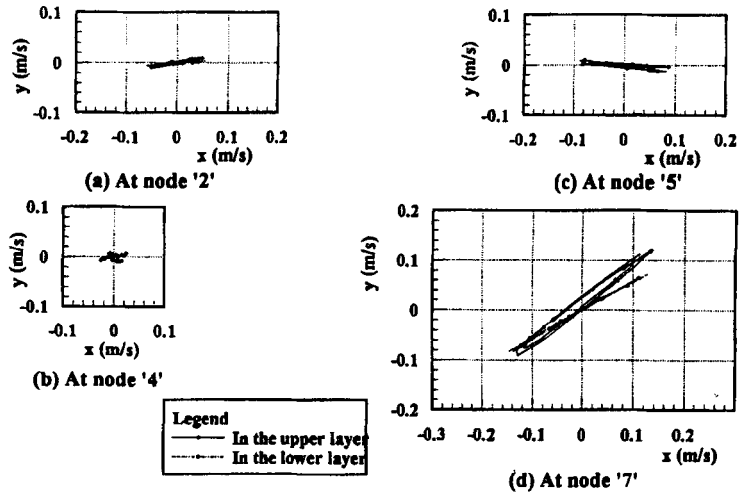

Figure 14. Computed velocity hodographs during 9–10 May 1983

5. CONCLUSIONS

Two-layer flow in which a lighter layer flows on a heavier lower layer is commonly encountered in practical situations. Significant advances have been achieved in research on such systems during the past two decades. This paper reports a new two-layer, two-dimensional mathematical model with a finite difference method based on numerically generated boundary-fitted orthogonal co-ordinates. It can be used to simulate flows with density stratification in a natural water-body with complicated

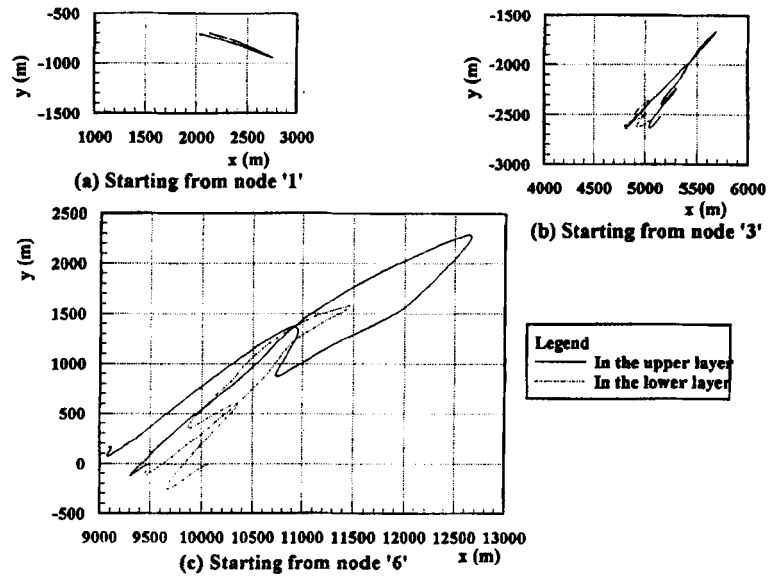

Figure 15. Computed Lagrangian pathlines during 16–17 May 1983

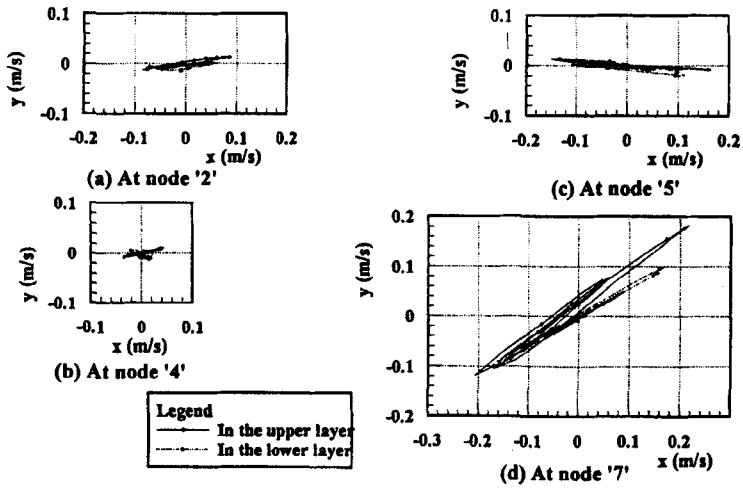

Figure 16. Computed velocity hodographs during 16–17 May 1983

topography. A grid 'block' technique has been used to deal with the unsteady boundary problem. A time-splitting scheme is employed in which the advection and diffusion parts of the momentum equations are solved with an implicit finite difference method in the first fractional step and then the propagation and remaining terms are solved also with an implicit finite difference method in the second fractional step.

A case study on a real bay—Tolo Harbour, Hong Kong—has been conducted using the present model. The computational results of tidal elevation and velocity are compared with the three available measured data sets for Tolo Harbour. Fairly good agreement is found between the simulated results and the measurements. However, the corresponding computational results of velocity with no density difference between the surface and bottom layers show large discrepancies with the measured data. It is proved that the density stratification plays an important role in the tidal circulation. The present model is successful in treating the turbulent exchange across the interface and can reproduce the two-layer, two-dimensional tidal flow in Tolo Harbour very well.

The computed velocity hodographs show that the Eulerian velocities in most of the harbour, especially in the outer area, i.e. in the Tolo Channel, have a prevailing direction along the channel; however, the prevailing directions in the surface layer are generally different from those in the bottom layer. Generally, the tidal circulations at various positions in each layer have different patterns and the features of the patterns are independent of the tidal type except for their scales. The computed Lagrangian pathlines show that the tidal excursion is dependent on the tidal type, especially in the inner harbour and side-coves; during neap tide it is very small and this should be seriously taken into account in research on pollutant transport.

The computations demonstrate that the present numerical scheme performs well. A very large time step (Δt) in the model run, far exceeding the CFL stability criterion constraint, can be used and the results do not show any unreasonable numerical oscillations. Besides, the model allows the specification of flexible initial conditions.

In subsequent work we plan to incorporate the simulation of temperature and salinity simultaneously to capture the density stratification and also to adopt a more sophisticated turbulence model to capture the interaction between turbulence and buoyancy and the mixing across the interface more reasonably. It is anticipated that the model will then have much better performance.

REFERENCES

1. B. H. Johnson, K. W. Kim, R. E. Heath, B. B. Hsieh and H. L. Butler, 'Validation of three-dimensional hydrodynamic model of Chesapeake Bay', *J. Hydraul. Eng., ASCE*, **119**, 2–20 (1993).
2. C. -S. Yih, *Stratified Flows*, Academic, New York, 1980.
3. S. B. Dalziel, 'Two-layer hydraulics, a functional approach', *J. Fluid Mech.*, **223**, 135–163 (1991).
4. M. B. Abbott, *Computational Hydraulics: Elements of the Theory of Free Surface Flows*, Ashgate, Boston, 1979.
5. W. Tan, *Shallow Water Hydrodynamics: Mathematical Theory and Numerical Solution for a Two-Dimensional System of Shallow Water Equations*, Elsevier, Amsterdam, 1992.
6. G. C. Hocking, 'Critical withdrawal from a two-layer fluid through a line sink', *J. Eng. Math.*, **25**, 1–11 (1991).
7. C. Kranenburg and J. D. Pietrzak, 'Internal lee waves in turbulent two-layer flow', *J. Hydraul. Eng., ASCE*, **115**, 1352–1370 (1989).
8. N. V. M. Odd and J. G. Rodger, 'Vertical mixing in stratified tidal flows', *J. Hydraul. Div., ASCE*, **103**, 337–351 (1978).
9. W. S. Lung and D. J. O'Connor, 'Two-dimensional mass transport in estuaries', *J. Hydraul. Eng., ASCE*, **110**, 1340–1357 (1984).
10. M. Arita and G. H. Jirka, 'Two-layer model of saline wedge. II: Prediction of mean properties', *J. Hydraul. Eng., ASCE*, **113**, 1249–1263 (1987).
11. R. Bermejo, 'Finite-element model of two-layer ocean circulation', *Int. j. numer. methods eng.*, **29**, 665–678 (1990).
12. P. J. Roache, *Computational Fluid Dynamics*, Hermosa, Albuquerque, NM, 1975.
13. J. F. Thompson, Z. U. A. Warsi and C. W. Mastin, *Numerical Grid Generation—Foundations and Applications*, Elsevier, New York, 1985.
14. H. S. Jin, Y. M. Zheng and J. Ye, 'A general mathematical model of tidal current in natural river', in R. A. Falconer *et al.* (eds), *Hydraulic and Environmental Modelling: Coastal Waters*, Ashgate, Brookfield, 1992, pp. 481–492.
15. W. Rodi, *Turbulence Models and Their Applications in Hydraulics, State-of-the-Art*, IAHR, Delft, 1980.
16. R. Franke, M. A. Leschziner and W. Rodi, 'Numerical simulation of wind-driven turbulent flow in stratified water bodies', in E. J. List and G. H. Jirka (eds), *Proc. Third Int. Symp. on Stratified Flows*, Pasadena, CA, February 1987, ASCE, New York, 1990, pp. 993–1004.
17. H. S. Jin and S. N. Zhang, 'A simplified turbulence stress/flux algebraic model and its application to stratified flows', in J. H. W. Lee and Y. K. Cheung (eds), *Proc. Int. Symp. on Environmental Hydraulics*, Hong Kong, December 1991, Balkema, Rotterdam, 1991, pp. 577–582.
18. G. T. Orlob, *Mathematical Modelling of Water Quality: Streams, Lakes, and Reservoirs*, Wiley–Interscience, New York, 1983.
19. P. Huang, J. L. DiLorenzo and T. O. Najarian, 'Mixed-layer hydrothermal reservoir model', *J. Hydraul. Eng., ASCE*, **120**, 846–862 (1994).
20. S. V. Patankar, *Numerical Heat Transfer and Fluid Flow*, Hemisphere, New York, 1980.
21. I. J. Hodgkiss and B. S. S. Chan, 'Pollution studies on Tolo Harbour, Hong Kong', *Marine Environ. Res.*, **10**, 1–44 (1983).
22. *Tolo Water Quality Model, Final Report*, Binnie & Partners, Hong Kong, 1984.
23. C. W. Li *et al.*, 'Mathematical model study of tidal circulation in Tolo Harbour, Hong Kong: development and verification of a semi-implicit finite element scheme', *Proc. Inst. Civil Eng.*, **81**, 569–592 (1986).
24. K. W. Choi, 'Finite difference modelling of estuarine hydrodynamics', *Master's Thesis*, University of Kong Kong, 1985.